Thermodynamic properties and phase diagram of quark matter within non-extensive Polyakov chiral *SU* (3) quark mean field model

Dhananjay Singh[†]   Arvind Kumar[‡]

Department of Physics, Dr. B R Ambedkar National Institute of Technology Jalandhar, Jalandhar – 144008, Punjab, India

Abstract: In the present study, we applied Tsallis non-extensive statistics to investigate the thermodynamic properties and phase diagram of quark matter in the Polyakov chiral *SU*(3) quark mean field model. Within this model, the properties of the quark matter were modified through the scalar fields $\sigma, \zeta, \delta, \chi$, vector fields ω, ρ, ϕ, and Polyakov fields Φ and $\bar{\Phi}$ at finite temperature and chemical potential. Non-extensive effects were introduced through a dimensionless parameter q, and the results were compared to those of the extensive case ($q \to 1$). In the non-extensive case, the exponential in the Fermi-Dirac (FD) function was modified to a q-exponential form. The influence of the q parameter on the thermodynamic properties, pressure, energy, and entropy density, as well as trace anomaly, was investigated. The speed of sound and specific heat with non-extensive effects were also studied. Furthermore, the effect of non-extensivity on the deconfinement phase transition as well as the chiral phase transition of u, d, and s quarks was explored. We found that the critical end point (CEP), which defines the point in the $(T - \mu)$ phase diagram where the order of the phase transition changes, shifts to a lower value of temperature, T_{CEP}, and a higher value of chemical potential, μ_{CEP}, as the non-extensivity is increased, that is, $q > 1$.

Keywords: quark matter, quark mean field model, QCD phase diagram, non-extensive statistics

DOI: 10.1088/1674-1137/ad2a64

I. INTRODUCTION

Quantum chromodynamics (QCD) is a theory of strong interactions among the fundamental constituents of matter: quarks and gluons. In the low energy regime (10^{-2} GeV), perturbative approaches to solve QCD became obsolete, and we had to rely on non-perturbative methods. This led to the development of two theoretical approaches to QCD, namely, lattice quantum chromodynamics (LQCD) and effective models of QCD. In LQCD, numerical techniques are applied on a discretized lattice of space and time. The discretization of space and time allows the equations to become computationally tractable to calculate the properties of hadrons and other QCD systems. Effective field models (EFMs) based on the effective field theory were also developed to investigate the low-energy regime of QCD. The EFM uses a simpler set of degrees of freedom than that of the underlying theory. Studying the thermodynamic properties and phase transition of quark matter at finite temperatures has always been a topic of great interest in high-energy physics. They play an important role in exploring physics shortly

after the Big Bang [1]. They are also relevant in studying the properties and structure of compact stars at high baryonic density and low temperature [2–6]. At low baryonic density and high temperature, they are relevant to explain the quark gluon plasma (QGP) formation in relativistic heavy-ion collisions [7]. Exploring the thermodynamic properties of dense quark matter is essential to understand the nature of the phase transition in the $(T - \mu_B)$ plane. The phase diagram of QCD contains information about the equilibrium phases of QCD and the physics of phase transition.

Many theoretical models have been used to study the properties of hot and dense quark matter. These include the quark-meson coupling (QMC) model [8, 9], Polyakov QMC (PQMC) model [10, 11], Nambu-Jona-Lasinio (NJL) model [12, 13], Polyakov NJL (PNJL) model [14, 15], linear sigma model (LSM) [16], Polyakov LSM (PLSM) [17–20], chiral *SU*(3) quark-mean-field (CQMF) model [21, 22], and Polyakov CQMF (PCQMF) model [23, 24]. However, the statistical approach used in these studies is often the standard Boltzmann-Gibbs (BG) statistics. The validation of BG statistics is limited to sys-

tems that satisfy the following conditions: short-range type interactions, homogeneous and infinite heat bath, weak or no correlations between elements, and smooth boundary conditions. Violation of one or more of these conditions questions the validation of BG statistics.

Consequently, Tsallis proposed non-extensive statistics, which depict a more realistic environment in heavy ion collision experiments. This formalism is an extension of the BG statistics [25]. In this framework, the usual exponential function is replaced by a $q-$exponential function [26, 27],

$$\exp_q(x) = [1 + (1-q)x]^{\frac{1}{1-q}}, \qquad (1)$$

where q is a dimensionless parameter called the non-extensive parameter and it contains all possible effects violating the standard BG statistics. Correspondingly, the logarithmic function is also modified to

$$\ln_q(x) = \frac{x^{1-q} - 1}{1-q}. \qquad (2)$$

Both functions return to their usual forms when $q \to 1$, that is, $\exp_q(x) \to \exp(x)$, $\ln_q(x) \to \ln(x)$, and Tsallis statistics returns to BG statistics. As the q parameter enters into the relevant formulae of the specific dynamical model, it enables the phenomenological examination of the stability of the model under consideration against potential departures from the BG approach. It must be emphasized here that Tsallis statistics is not an alternative but a generalization of BG statistics.

The motivation for this research comes from recent non-extensive statistics studies that showed the violation of BG statistics in high energy physics. There is considerable agreement between experimental data and theoretical models based on non-extensive effects. As shown in [28, 29], BG statistics failed to reproduce the freeze-out parameters. Tsallis statistics has also been proven to accurately produce the transverse momentum distributions that follow a power law distribution rather than an exponential distribution as in BG statistics [30–34]. Ref. [35] shows that Tsallis statistics can be used to explain the transport behaviour of cold atoms in optical lattices. Tsallis statistics also describes the behaviour of a system where ergodicity breaks down [36, 37]. The experimental data produced by the PHENIX [38], STAR [39], and RHIC collaborations by ATLAS [40] and ALICE [41] as well as collaborations at the LHC by the CMS [42] match very well within the framework of Tsallis statistics. Several authors have summarized the validation of non-extensive effects in high-energy physics as well as in astrophysics [43–56]. More details and diverse applications of Tsallis statistics can be found in [57].

The purpose of this study was to investigate a strongly interacting system whose dynamics are governed by non-extensive statistics. We investigated the difference between the thermodynamic properties of quark matter when Tsallis statistics is applied and those with BG statistics. We also studied the phase transition of quark matter within the realm of non-extensive statistics. For this, we generalized the PCQMF model to its non-extensive version. We explored situations where both the chemical potential and temperature are non zero, which stipulate the effect of Tsallis statistics on the whole $(T - \mu_B)$ plane in the phase diagram. Other models, such as the QHD model, have also been generalized to their non-extensive version to study the properties of nuclear matter [58]. Non-extensive statistical effects on the properties of quark matter have also been studied within a generalized NJL model [59]. Furthermore, a generalized version of the MIT bag model has also been used to study the QCD phase diagram and stellar matter properties [60]. In Ref. [61], a non-extensive linear sigma model was used to study the chiral phase transition. Recently, the PNJL model was also generalized to its non-extensive version to study the thermodynamic properties and transport coefficients [26], phase transition, and critical exponents of QCD matter [62], and baryon number fluctuations [63]. Moreover, non-extensive statistics have also been used to study fluctuations and correlations in high-energy nuclear collisions [44]. In Ref. [64], non-extensive effects were considered to study the relativistic nuclear equation of state. Ref. [65] included non-extensive effects to study the hadron to QGP transition. The bulk properties of protoneutron stars have also been investigated using the non-extensive formalism [66]. Non-extensive thermodynamics of nuclear matter, as well as a black hole, were studied in [67]. Moreover, in Ref. [68] non-extensive effects were used to study the transport properties of hadronic matter.

The rest of this paper is organized as follows. In Sec. II, we introduce the non-extensive version of the Polyakov chiral $SU(3)$ quark mean field model (q-PCQMF). The impact of the non-extensive parameter q on various thermodynamic properties of quark matter is discussed in Sec. III.A. In Sec. III.B, we analyze in detail the influence of the parameter q on the chiral and deconfinement phase transition at finite quark chemical potential and finite temperature. Finally, in Sec. IV, we provide a brief summary of our work.

II. POLYAKOV CHIRAL *SU*(3) QUARK MEAN FIELD MODEL

Before presenting the q-PCQMF model, let us introduce the main concepts of the PCQMF model. This model uses quarks and mesons as degrees of freedom. At finite temperature and density, the interactions between quarks in this model are described by the exchange of the

scalar meson fields σ, ζ, and δ and vector meson fields ω, ρ, and ϕ. The Polyakov fields Φ and $\bar{\Phi}$ are introduced in the model to study the features of the deconfinement phase transition. The attractive part of the interaction is represented by the scalar meson fields, whereas the repulsive interaction is represented by the vector meson fields. The non-strange scalar isoscalar meson field σ corresponds to the scalar meson of mass 417 MeV [22] and has $(u\bar{u}/d\bar{d})$ as its content. The scalar meson interacts with the strange quark through a strange scalar isoscalar field, ζ, with $(s\bar{s})$ as its content and a mass of 1170 MeV [22]. The scalar isovector field δ is introduced in the model to study the effect of isospin asymmetry and has $(u\bar{u}-d\bar{d})$ as its content. Furthermore, the model introduces the broken scale invariance through a scalar dilaton field, χ, also known as glueball field [69–73].

The effective Lagrangian of 2 + 1 flavour and 3 colour PCQMF model is as follows:

$$\mathcal{L}_{\text{PCQMF}} = \mathcal{L}_{q0} + \mathcal{L}_{qm} + \mathcal{L}_{M} + \mathcal{L}_{\Delta m} + \mathcal{L}_{h} - U(\Phi(\vec{x}), \bar{\Phi}(\vec{x}), T). \tag{3}$$

In the above equation, $\mathcal{L}_{q0} = \bar{\psi} i \gamma^\mu \partial_\mu \psi$ represents the free part of massless quarks. The interactions between quark and meson is represented by

$$\mathcal{L}_{qm} = g_s \left(\bar{\psi}_L M \psi_R + \bar{\psi}_R M^+ \psi_L \right) - g_v \left(\bar{\psi}_L \gamma^\mu l_\mu \psi_L + \bar{\psi}_R \gamma^\mu r_\mu \psi_R \right), \tag{4}$$

where $\psi = (u, d, s)$ and $g_v(g_s)$ are vector(scalar) coupling constants. The spin-0 scalar (Σ) and pseudoscalar (Π) mesons are expressed as [74]

$$M(M^\dagger) = \Sigma \pm i\Pi = \frac{1}{\sqrt{2}} \sum_{a=0}^{8} (\sigma^a \pm i\pi^a) \lambda^a, \tag{5}$$

where $\sigma^a(\pi^a)$ represent the scalar (pseudoscalar) meson nonets and λ^a are the Gell-Mann matrices with $\lambda^0 = \sqrt{\frac{2}{3}} \mathbb{1}$. Similarly, the spin-1 vector (V_μ) and pseudovector (A_μ) mesons are expressed as [74]

$$l_\mu(r_\mu) = \frac{1}{2}(V_\mu \pm A_\mu) = \frac{1}{2\sqrt{2}} \sum_{a=0}^{8} (v_\mu^a \pm a_\mu^a) \lambda^a, \tag{6}$$

with v_μ^a (a_μ^a) being vector (pseudovector) mesons nonets.

The meson interactions are described by the term $\mathcal{L}_M = \mathcal{L}_{\Sigma\Sigma} + \mathcal{L}_{VV} + \mathcal{L}_{SB}$. The self-interaction term for the scalar meson in the mean field approximation can be expressed as

$$\begin{aligned}
\mathcal{L}_{\Sigma\Sigma} = &-\frac{1}{2} k_0 \chi^2 \left(\sigma^2 + \zeta^2 + \delta^2 \right) \\
&+ k_1 \left(\sigma^2 + \zeta^2 + \delta^2 \right)^2 + k_2 \left(\frac{\sigma^4}{2} + \frac{\delta^4}{2} + 3\sigma^2\delta^2 + \zeta^4 \right) \\
&+ k_3 \chi \left(\sigma^2 - \delta^2 \right) \zeta - k_4 \chi^4 - \frac{1}{4} \chi^4 \ln \frac{\chi^4}{\chi_0^4} \\
&+ \frac{d}{3} \chi^4 \ln \left(\left(\frac{(\sigma^2 - \delta^2) \zeta}{\sigma_0^2 \zeta_0} \right) \left(\frac{\chi^3}{\chi_0^3} \right) \right),
\end{aligned} \tag{7}$$

where $d = 6/33$; σ_0 and ζ_0 correspond to the vacuum values of the σ and ζ fields, respectively. These are expressed as $\sigma_0 = -f_\pi = 93$ MeV and $\zeta_0 = (f_\pi - 2f_K)/\sqrt{2} = 115$ MeV, where f_π is the pion decay constant and f_K is the kaon decay constant.

The self-interaction term for the vector meson is written as

$$\begin{aligned}
\mathcal{L}_{VV} = &\frac{1}{2} \frac{\chi^2}{\chi_0^2} \left(m_\omega^2 \omega^2 + m_\rho^2 \rho^2 + m_\phi^2 \phi^2 \right) \\
&+ g_4 \left(\omega^4 + 6\omega^2\rho^2 + \rho^4 + 2\phi^4 \right),
\end{aligned} \tag{8}$$

where the density-dependence of the mass of the vector meson can be written as [75]

$$m_\omega^2 = m_\rho^2 = \frac{m_v^2}{1 - \frac{1}{2}\mu\sigma^2}, \quad \text{and} \quad m_\phi^2 = \frac{m_v^2}{1 - \mu\zeta^2}. \tag{9}$$

The parameters $m_v = 673.6$ MeV and density $\mu = 2.34$ fm^2 are taken to yield $m_\phi = 1020$ MeV and $m_\omega = 783$ MeV.

The masses of pseudo-scalar mesons arise owing to the term [74, 76, 77]

$$\mathcal{L}_{SB} = -\frac{\chi^2}{\chi_0^2} \left[m_\pi^2 f_\pi \sigma + \left(\sqrt{2} m_K^2 f_K - \frac{m_\pi^2}{\sqrt{2}} f_\pi \right) \zeta \right]. \tag{10}$$

The exact mass of the s quark is generated through $\mathcal{L}_{\Delta m} = -\Delta m_s \bar{\psi} S \psi$, where $\Delta m_s = 29$ MeV and $S = \frac{1}{3} \left(I - \lambda_8 \sqrt{3} \right) = \text{diag}(0, 0, 1)$.

To study the dependence of T and μ_B in this model, we investigated the grand canonical potential density, which can be expressed in the mean field approximation as

$$\begin{aligned}
\Omega_{\text{PCQMF}} = &\mathcal{U}(\Phi, \bar{\Phi}, T) - \mathcal{L}_M - \mathcal{V}_{vac} \\
&+ \sum_{i=u,d,s} \frac{-\gamma_i k_B T}{(2\pi)^3} \int_0^\infty \mathrm{d}^3 k \left\{ \ln F^- + \ln F^+ \right\},
\end{aligned} \tag{11}$$

where $\gamma_i = 2$ is the spin degeneracy factor, and

$$F^- = 1 + e^{-3E^-} + 3\Phi e^{-E^-} + 3\bar{\Phi} e^{-2E^-}, \tag{12}$$

$$F^+ = 1 + e^{-3E^+} + 3\bar{\Phi} e^{-E^+} + 3\Phi e^{-2E^+}. \tag{13}$$

In the above equations, $E^- = (E_i^*(k) - \nu_i^*)/k_B T$ and $E^+ = (E_i^*(k) + \nu_i^*)/k_B T$, in which the effective single particle energy of quarks is given by $E_i^*(k) = \sqrt{m_i^{*2} + k^2}$. In Eq. (11), the term $\mathcal{V}_{vac}$ is subtracted for the sake of obtaining zero vacuum energy. The in-medium quark chemical potential ν_i^* is linked to the chemical potential ν_i in free space by

$$\nu_i^* = \nu_i - g_\omega^i \omega - g_\phi^i \phi - g_\rho^i \rho, \tag{14}$$

where g_ω^i, g_ϕ^i, and g_ρ^i are the coupling constants of vector meson fields with different quarks. The effective mass of the quark, m_i^*, is given by

$$m_i^* = -g_\sigma^i \sigma - g_\zeta^i \zeta - g_\delta^i \delta + m_{i0}, \tag{15}$$

where g_σ^i, g_ζ^i, and g_δ^i describe the coupling strength of scalar fields with different quarks. The values of g_σ^i, g_ζ^i, and m_{i0} are determined by fitting the vacuum masses of the constituent quarks, $m_u, m_d, m_s = 313$ MeV, 313 MeV, 490 MeV, respectively [75].

For the Polyakov loop effective potential, we considered the commonly used logarithmic form given by [14, 78, 79]

$$\frac{U(\Phi, \bar{\Phi}, T)}{T^4} = -\frac{a(T)}{2} \bar{\Phi}\Phi$$
$$+ b(T)\ln\left[1 - 6\bar{\Phi}\Phi + 4(\bar{\Phi}^3 + \Phi^3) - 3(\bar{\Phi}\Phi)^2\right], \tag{16}$$

with the temperature dependent coefficients [78, 80]

$$a(T) = a_0 + a_1\left(\frac{T_0}{T}\right) + a_2\left(\frac{T_0}{T}\right)^2, \quad b(T) = b_3\left(\frac{T_0}{T}\right)^3. \tag{17}$$

The corresponding parameters a_0, a_1, a_2, and b_3 are presented in Table 1.

In the pure gauge sector at vanishing chemical potential, the parameter $T_0 = 270$ MeV [81]. T_0 is rescaled from 270 to 200 MeV when fermionic fields are included to compare the model results with existing lattice results [23]. Finally, the solutions of the scalar fields σ, ζ, and δ, the dilaton field χ, the vector fields ω, ρ, and ϕ, and the Polyakov field Φ and its conjugate $\bar{\Phi}$ are obtained by minimizing Ω with respect to these fields, *i.e.*,

$$\frac{\partial\Omega}{\partial\sigma} = \frac{\partial\Omega}{\partial\zeta} = \frac{\partial\Omega}{\partial\delta} = \frac{\partial\Omega}{\partial\chi} = \frac{\partial\Omega}{\partial\omega} = \frac{\partial\Omega}{\partial\rho} = \frac{\partial\Omega}{\partial\phi} = \frac{\partial\Omega}{\partial\Phi} = \frac{\partial\Omega}{\partial\bar{\Phi}} = 0. \tag{18}$$

The model parameters, which are summarized in Table 2, can be estimated using the masses of the π, K mesons, average masses of η and η', and vacuum masses of the σ, ζ, and χ mesons.

A. *q*-PCQMF model

The PCQMF model assumes the additivity of some thermodynamical quantities such as entropy. For systems where long-range correlations and fluctuations are important, for example, under phase transition, this is a very strong approximation. One way to take the nonadditivity of interacting systems into account is to consider a microcanonical ensemble of Hamiltonian systems [82, 83]. An alternative approach is to make use of Tsallis statistics [25]. As discussed in Sec. I, a promising possibility consists of resigning from the assumption of additivity and describing the theoretical models based on the non-extensive approach. In this spirit, we have extended the PCQMF model to its non-extensive version by using Tsallis statistics instead of BG statistics, which implies the replacements described in Eq. (1) and (2). However, we have taken the following simplifications. First, the

Table 1. Parameters in the Polyakov effective potential.

a_0	a_1	a_2	b_3
1.81	−2.47	15.2	−1.75

Table 2. List of parameters used in the present work.

k_0	k_1	k_2	k_3	k_4	g_s	g_v	g_4	h_1	h_2
4.94	2.12	−10.16	−5.38	−0.06	4.76	10.92	37.5	0	0

σ_0/MeV	ζ_0/MeV	χ_0/MeV	m_π/MeV	f_π/MeV	m_K/MeV	f_K/MeV	m_ω/MeV	m_ϕ/MeV	m_ρ/MeV
−93	−96.87	254.6	139	93	496	115	783	1020	783

g_σ^u	g_σ^d	g_σ^s	g_ζ^u	g_ζ^d	g_ζ^s	g_δ^u	g_δ^d	g_δ^s	ρ_0/fm^{-3}
3.36	3.36	0	0	0	4.76	3.36	−3.36	0	0.15

g_ω^u	g_ω^d	g_ω^s	g_ϕ^u	g_ϕ^d	g_ϕ^s	g_ρ^u	g_ρ^d	g_ρ^s	d
3.86	3.86	0	0	0	5.46	3.86	−3.86	0	0.18

Polyakov loop potential experiences non-extensive effects only implicitly and hence remains unchanged. Second, similar to the case of finite-size effects where the volume V is treated on the same footing as T and μ [24], the usual parameters of the PCQMF model are left undisturbed, and the q parameter is treated on the same footing as T and μ.

Hence, within the q-PCQMF model, the thermodynamic potential density becomes

$$\Omega_q = \mathcal{U}(\Phi,\bar{\Phi},T) - \mathcal{L}_M - \mathcal{V}_{vac} \\ + \sum_{i=u,d,s} \frac{-\gamma_i k_B T}{(2\pi)^3} \int_0^\infty \mathrm{d}^3k \left\{ \ln_q F_q^- + \ln_q F_q^+ \right\}, \quad (19)$$

where

$$F_q^- = 1 + e_q(-3E^-) + 3\Phi e_q(-E^-) + 3\bar{\Phi}e_q(-2E^-), \quad (20)$$

$$F_q^+ = 1 + e_q(-3E^+) + 3\bar{\Phi}e_q(-E^+) + 3\Phi e_q(-2E^+). \quad (21)$$

The coupled equations obtained by minimizing Ω_q in Eq. (19) are given in the appendix. The q versions of vector density, ρ_i, and scalar density, $\rho_{q,i}^s$, of quarks are written as

$$\rho_i = \gamma_i N_c \int \frac{\mathrm{d}^3k}{(2\pi)^3} \left(f_{q,i}(k) - \bar{f}_{q,i}(k) \right), \quad (22)$$

and

$$\rho_i^s = \gamma_i N_c \int \frac{\mathrm{d}^3k}{(2\pi)^3} \frac{m_i^*}{E_i^*(k)} \left(f_{q,i}(k) + \bar{f}_{q,i}(k) \right), \quad (23)$$

respectively, where $f_{q,i}(k)$ and $\bar{f}_{q,i}(k)$ are the q-modified Fermi-distribution functions for the quark and anti-quark at finite temperature and are given by

$$f_{q,i}(k) = \frac{\Phi e_q^q(-E^-) + 2\bar{\Phi}e_q^q(-2E^-) + e_q^q(-3E^-)}{[1 + 3\Phi e_q(-E^-) + 3\bar{\Phi}e_q(-2E^-) + e_q(-3E^-)]^q}, \quad (24)$$

$$\bar{f}_{q,i}(k) = \frac{\bar{\Phi}e_q^q(-E^+) + 2\Phi e_q^q(-2E^+) + e_q^q(-3E^+)}{[1 + 3\bar{\Phi}e_q(-E^+) + 3\Phi e_q(-2E^+) + e_q(-3E^+)]^q}. \quad (25)$$

It is important to note that, in the limit $q \to 1$, the standard Fermi-distribution functions are recovered, and hence, we return to the standard (extensive) PCQMF model.

The following restriction must hold for $e_q(x)$ to always be a non-negative real function:

$$[1 + (1-q)x] \geq 0. \quad (26)$$

In this study, we consider only $q > 1$. This is because it was discovered that the typical value of the non-extensivity parameter q for high-energy collisions is $1 \leq q \leq 1.2$ [31, 32, 84, 85]. Furthermore, for $q > 1$, $q-1$ describes intrinsic fluctuations of temperature in the system [47, 49], whereas the interpretation of $q-1$ for $q < 1$ is inconsistent [86, 87]. To comply with Eq. (26), for $q > 1$, we can use the following Tsallis cutoff prescription [88]:

$$e_q(x) = \begin{cases} [1 + (1-q)x]^{\frac{1}{1-q}}, & \text{for} \quad x \leq 0, \\ [1 + (q-1)x]^{\frac{1}{q-1}}, & \text{for} \quad x > 0. \end{cases} \quad (27)$$

In addition, let us observe that, as $T \to 0$, as long as $q > 1$, $\Omega_q \to \Omega$ and the non-extensive effects vanish. This means that in studies where in the nuclear scale $T \approx 0$ (in the interior of neutron stars) we expect no non-extensive signature. However, when T is in MeVs, (heavy-ion collision experiments), one expects the non-extensive effects to play an important role in the thermodynamic quantities. To study such effects, we applied the modified thermodynamic potential density Eq. (19) in Eq. (18) to calculate the in-medium q-value of the vector and scalar fields. The isospin asymmetry can be incorporated through the definition $\eta = \frac{(\rho_d - \rho_u)}{(\rho_d + \rho_u)/3}$. The total baryon density is given by $\rho_B = (\rho_u + \rho_d + \rho_s)/3$. The various chemical potentials are defined through $\mu_B = 3(\mu_u + \mu_d)/2$, $\mu_I = (\mu_u - \mu_d)/2$, and $\mu_S = (\mu_u + \mu_d - 2\mu_s)/2$, corresponding to the baryon, isospin, and strangeness chemical potentials, respectively.

III. RESULTS AND DISCUSSIONS

In this section, we present various results on the thermodynamical properties of quark matter within the q−extended Polyakov chiral $SU(3)$ quark mean-field model (q-PCQMF) presented in Sec. II.A. In the q-PCQMF model, the effect of the q parameter comes into the picture through the thermodynamic potential density, Ω_q, which depends upon the q−dependent scalar density ρ_i^s and vector density ρ_i of the constituent quarks, which in turn depend upon the scalar fields ($\sigma, \zeta, \delta, \chi$), vector fields ($\omega, \rho, \phi$), and Polyakov loop fields, ($\Phi, \bar{\Phi}$). As stated before, these fields are calculated by solving the coupled system of non-linear equations. In Sec. III.A, the in-medium properties of the scalar and Polyakov loop fields are discussed. These fields will be used as input to understand the effect of q on different thermodynamic properties of quark matter. We will discuss the behaviour of the susceptibility of these fields and study the $(T - \mu)$ phase diagram and the influence of the q parameter on these quantities in Sec. III.B.

A. In-medium fields and thermodynamic properties

In Fig. 1, the variations of the scalar fields σ and ζ as well as the Polyakov fields Φ and $\bar{\Phi}$ are shown as a function of temperature, T, for $q = 1$, 1.05, and 1.10 at the baryon chemical potential $\mu_B = 400$ MeV, isospin chemical potential $\mu_I = 40$ MeV, and strangeness chemical potential $\mu_S = 125$ MeV. We observe that the magnitudes of σ and ζ decrease with an increase in temperature. The temperature at which the magnitude of the scalar fields begins to decrease rapidly is referred to as pseudo-critical temperature, T_p. This decrease in the magnitude of the scalar fields may represent the restoration of chiral symmetry at high temperatures. Here, we can see that as q increases, the value of T_p decreases. As the temperature is increased, the Fermi distribution function in Eqs. (24) and (25) decreases resulting in a decrease in the magnitude of the scalar fields. At higher values of q, there is a considerable decrease in the magnitude of the fields, even at lower temperatures. This may signify that the transition temperature is shifted towards a lower temperature value.

In the mean-field approximation, the order parameters to study the deconfinement are the Polyakov loop fields, Φ and $\bar{\Phi}$. The variation in the magnitude of Φ and $\bar{\Phi}$ provides information about the deconfinement phase transition. As can be observed in Fig. 1 (c) and (d), at lower temperatures, the value of both Φ and $\bar{\Phi}$ is approximately zero, indicating confined quarks within hadrons. With an increase in temperature, Φ and $\bar{\Phi}$ increase and reach a critical temperature, where it jumps to a non-zero value, indicating the deconfinement phase transition. Similar to the scalar fields, we find that, as non-extensivity increases (higher values of q), this increase in Φ and
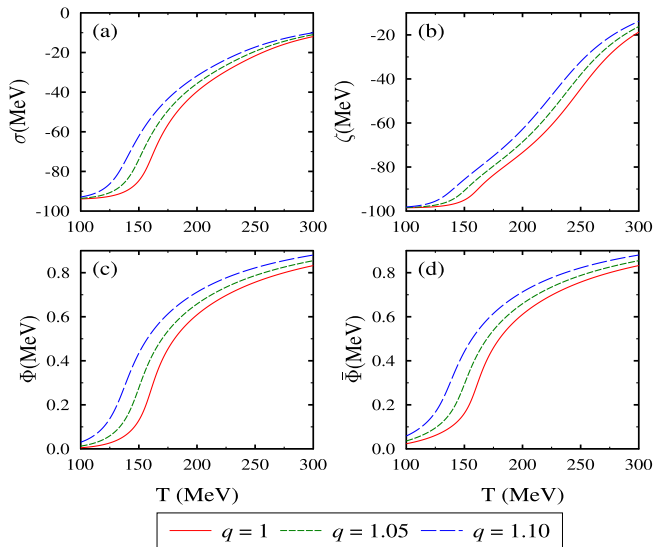
$\bar{\Phi}$ occurs earlier. This may indicate a decrease in the deconfinement temperature for $q > 1$.

One can calculate various thermodynamic properties such as energy density, pressure density, entropy density, and trace anomaly of quark matter with the help of the thermodynamics potential density, Ω_q, in Eq. (19). The pressure is given by

$$p_q(T) = -\Omega_q(T). \tag{28}$$

The entropy density and energy density are given by

$$s_q(T) = -\frac{\partial\Omega_q(T)}{\partial T}, \qquad \epsilon_q(T) = \Omega_q(T) + \sum_{i=u,d,s} \nu_i^* \rho_i + T s_q(T), \tag{29}$$

respectively.

Figure 2 shows the behaviour of ϵ_q/T^4, p_q/T^4, s_q/T^3, and $(\epsilon_q - 3p_q)/T^4$ at $\mu_B = 400$ MeV, $\mu_I = 40$ MeV, and $\mu_S = 125$ MeV for $q = 1, 1.05$, and 1.10. All these quantities show smooth behaviour implying a crossover phase transition. We see a sharp increase in the value of these quantities near the transition temperature. It is interesting to note that when $q = 1$, these thermodynamic quantities all tend to their Stefan Boltzmann (SB) limit at higher temperatures. However, with an increase in q, they increase rapidly and exceed their corresponding SB limit. For ϵ_q/T^4 at $T = 300$ MeV, the value at $q = 1$ is 14.39 (very close to the SB limit, 15.627) but as q is increased to 1.1, its value increases by 75% to 25.24. For s_q/T^3 and p_q/T^4, these values are 80% and 105%, respectively. This is the anticipated result in the q−PCQMF model, because of the usage of Tsallis statistics instead of BG statistics. In Tsallis statistics, $q − 1$ is interpreted as a deviation from the BG statistics [47, 89]. The higher the value of $q − 1$, the greater the deviation from the BG statistics, and correspondingly, the higher the value of the SB limit for quark matter. This is because when $T \to \infty$, the modified thermodynamic potential density does not return to its normal value, that is, $\Omega_q \neq \Omega$. This means that, for a system whose dynamics are described by Tsallis statistics, the high-temperature limit of various thermodynamic quantities is no longer the SB limit but a q-dependent Tsallis limit. This is similar to the results obtained from the q-NJL model [26].

Some other relevant quantities in relativistic heavy-ion collision are the speed of sound squared at constant entropy c_{sq}^2 and specific heat at constant volume c_{vq}, which are defined as

$$c_{sq}^2 = \left(\frac{\partial p_q}{\partial \epsilon_q}\right)_{s_q} = \frac{s_q}{c_{vq}}, \qquad c_{vq} = \left(\frac{\partial \epsilon_q}{\partial T}\right)_V. \tag{30}$$
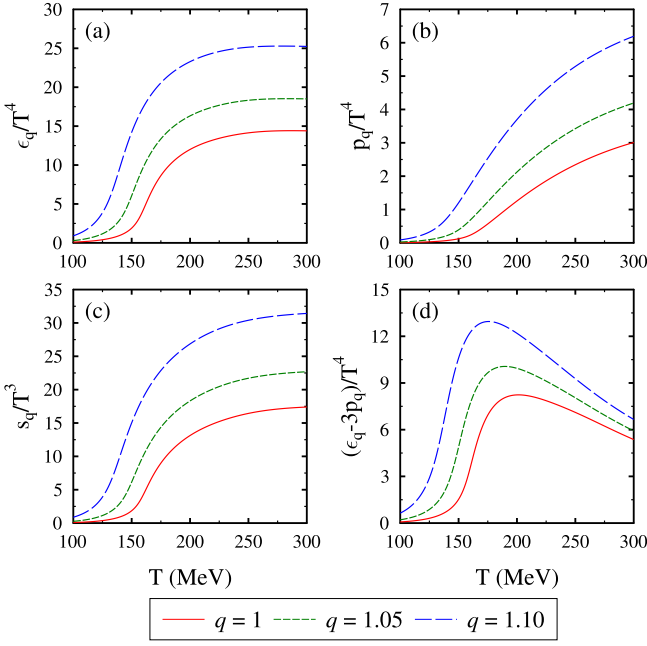

Fig. 1. (color online) Scalar fields σ and ζ and Polyakov fields Φ and $\bar{\Phi}$ plotted as a function of temperature T, for $q = 1$, 1.05, and 1.10 at $\mu_B = 400$ MeV, $\mu_I = 40$ MeV, and $\mu_S = 125$ MeV.

Fig. 2. (color online) Scaled energy density, ϵ_q/T^4, pressure density, p_q/T^4, entropy density, s_q/T^3, and trace anomaly, $(\epsilon_q - 3p_q)/T^4$ as a function of temperature T, for $q = 1$, 1.05, and 1.10 at $\mu_B = 400$ MeV, $\mu_I = 40$ MeV, and $\mu_S = 125$ MeV.
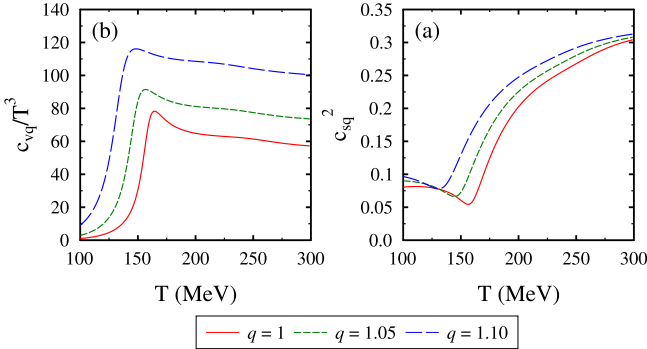

Fig. 3. (color online) Scaled specific heat, c_{vq}/T^3, and square of the speed of sound, c_{sq}^2, as a function of temperature T, for $q = 1$, 1.05, and 1.10 at $\mu_B = 400$ MeV, $\mu_I = 40$ MeV, and $\mu_S = 125$ MeV.

From Fig. 3 (a), we can observe that the value of c_{vq}/T^3 shows a trend similar to that of the other thermodynamic quantities discussed above. At $q = 1$, its value increases with an increase in temperature, reaches a maximum near the pseudo-critical temperature, and then tends to the usual SB limit, 63.14. Moreover, for higher values of q, it also reaches a new q-dependent Tsallis limit. In Fig. 3 (b), at $q = 1$, the value of c_{sq}^2 dips near the pseudo-critical temperature but then approaches the SB value, 0.33. However, as q increases, the dip disappears and the criticality vanishes. It is interesting to note that at high temperatures, both s_q/T^3 and c_{vq}/T^3 show similar growth. Therefore, non-extensive effects such as a high-temperat-

ure limit are not observed in $c_{sq}^2 = \frac{s_q}{T^3} / \frac{c_{vq}}{T^3}$. Similar results are obtained in Ref. [90].

B. $T - \mu$ phase diagram

In this subsection, we study the $T - \mu$ phase diagram within the q-PCQMF model. We analyze three phase transitions in the present study: the chiral phase transition from the chirally broken phase to the chiral restoration phase for up and down quarks, the chiral phase transition for the strange quark, and the deconfinement phase transition. The effect of the q parameter on the nature of these phase transitions is studied with the help of the susceptibilities, defined as

$$\chi_{\sigma_x} = \left(\frac{\partial \sigma_x}{\partial T} \right)_\mu, \quad \chi_{\sigma_y} = \left(\frac{\partial \sigma_y}{\partial T} \right)_\mu,$$

$$\chi_\Phi = \left(\frac{\partial \Phi}{\partial T} \right)_\mu, \quad \chi_{\bar\Phi} = \left(\frac{\partial \bar\Phi}{\partial T} \right)_\mu, \tag{31}$$

where σ_x for the u and d quarks and σ_y for the s quark are the scalar quark condensates, which can be expressed in terms of scalar fields $\sigma, \zeta, \delta,$ and $\chi,$ as follows [23]:

$$\sigma_x = \sigma_{u,d} = \frac{1}{m_{u,d}} \left(\frac{\chi}{\chi_0} \right)^2 \left[\frac{1}{2} m_\pi^2 f_\pi (\sigma \pm \delta) \right], \tag{32}$$

$$\sigma_y = \frac{1}{m_s} \left(\frac{\chi}{\chi_0} \right)^2 \left[\left(\sqrt{2} m_k^2 f_k - \frac{1}{\sqrt{2}} m_\pi^2 f_\pi \right) \zeta \right]. \tag{33}$$

From Fig. 1, it is evident that there is a smooth transition of the order parameters (scalar fields (σ and ζ) and Polyakov loop (Φ and $\bar\Phi$)). We do however see a change in the behaviour of these order parameters as we increase the temperature. This is evidence of a crossover phase transition, and we can study the susceptibilities defined in Eq. (31) to determine the position of the pseudo-critical point T_p. The peak values of the susceptibilities $\chi_{\sigma_x}, \chi_{\sigma_y}$ correspond to the pseudo-critical temperatures T_χ^q, T_χ^s for the chiral phase transition of up/down and strange quarks, respectively. The pseudo-critical temperature for the deconfinement phase transition T_d is obtained through χ_Φ. Figure 4 shows the variation of susceptibilities, χ_{σ_x}, for up and down quarks, χ_{σ_y}, for the strange quark, and the Polyakov loop, χ_Φ and $\chi_{\bar\Phi}$ at $\mu_B = 400, \mu_I = 40, \mu_S = 125$ MeV for $q = 1, 1.05,$ and 1.10. For $q = 1$, χ_{σ_x} shows a peak at $T \approx 160$ MeV, whereas χ_{σ_y} has two peaks, one at $T \approx 160$ MeV and another around $T \approx 247$ MeV. Furthermore, only a single peak, which coincides with the peak of χ_{σ_x} at $T \approx 160$ MeV, is observed for χ_Φ and $\chi_{\bar\Phi}$ at $q = 1$. The peak of the susceptibility gives us the pseudo-critical temperature. In the case of two peaks in susceptibilities, the criteria for deciding the pseudo-critical tem-

perature for chiral phase transition is given by $\sigma_{x,y}(T=0) < 1/2$, and for the deconfinement phase transition is $\Phi(T)/\Phi(T \to \infty) > 1/2$ [91]. It is evident from Fig. 4 that the values of these pseudo-critical temperatures decrease with increasing q for both the chiral phase transition T_χ^q and the deconfinement phase transition T_d. It is also interesting to note that the chiral phase transition for the strange quark occurs at a much higher temperature as evidenced by the second peak at $T_\chi^s \approx 247$ MeV, whereas for lighter up and down quarks, it occurs at $T_\chi^q \approx 160$ MeV.

The nature of the phase transition at a higher value of quark chemical potential is explored using quark number susceptibility. The chiral phase transition changes from a crossover to a first-order phase transition at higher values of μ_q, and this can be found by studying the discontinuity in the quark number density, ρ_u, or divergence in the corresponding susceptibility, χ_u, defined as

$$\chi_u = \left(\frac{\partial \rho_u}{\partial \mu}\right)_T. \tag{34}$$

In Fig. 5(a), the quark number density is plotted as a function of quark chemical potential for different values of temperature and zero vector interaction, at $q = 1$. It can be observed that, when $T \le T_{\text{CEP}}$, ρ_u shows a discontinuity, which can be seen in the corresponding susceptibility, χ_u, plotted in Fig. 5 (b), indicating the presence of first-order phase transition. When the temperature rises above T_{CEP}, the discontinuity in ρ_u disappears suggesting that
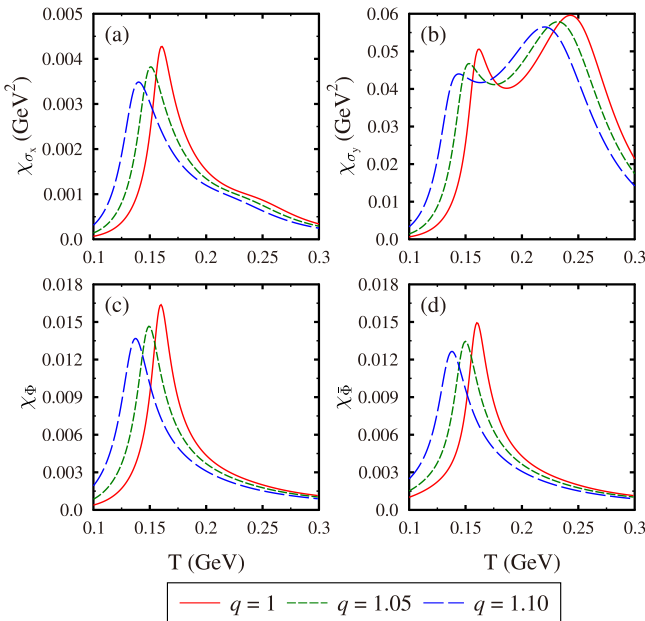
the order of the phase transition is a crossover. This change in the nature of ρ_u can be used to determine the location of the CEP. For $q = 1$, we observed the position of the CEP at approximately $(T, \mu) = (90$ MeV, 286 MeV) [23]. When the value of q is increased to 1.05, the peak in the χ_u is shifted towards higher μ and lower T, as shown
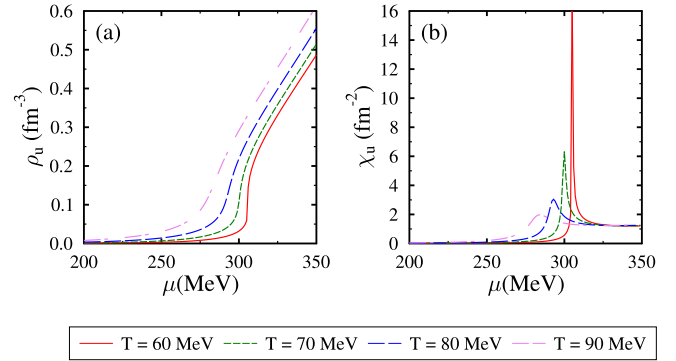

Fig. 5. (color online) Quark number density ρ_u and susceptibility χ_u of the up quark as a function of quark chemical potential at T = 70, 80, 90, and 100 MeV for $q = 1$.
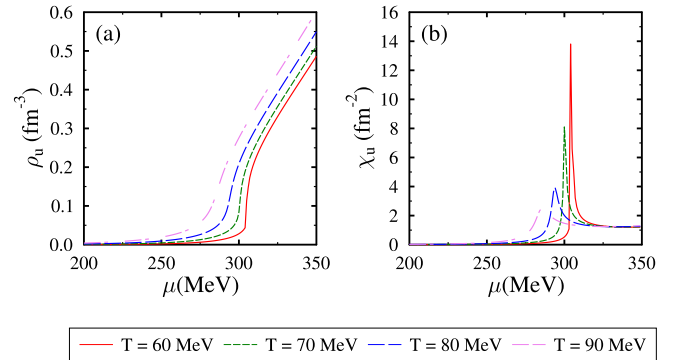

Fig. 6. (color online) Quark number density ρ_u and susceptibility χ_u of the up quark as a function of quark chemical potential at T = 70, 80, 90, and 100 MeV for $q = 1.05$.
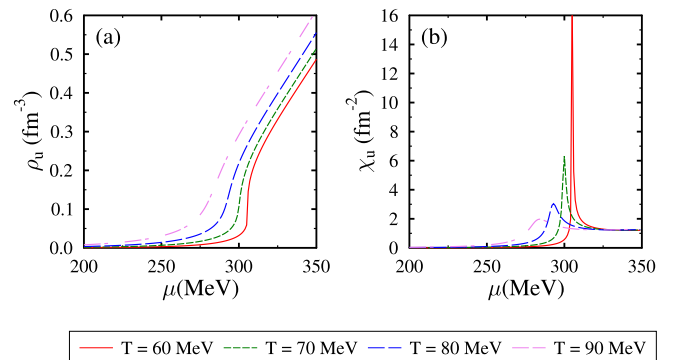

Fig. 7. (color online) Quark number density ρ_u and susceptibility χ_u of the up quark as a function of quark chemical potential at T = 70, 80, 90, and 100 MeV for $q = 1.10$.

Fig. 4. (color online) Susceptibilities of σ_x, σ_y, Φ, and $\bar{\Phi}$ at $q = 1$, 1.05, and 1.10 for $\mu_B = 400$ MeV, $\mu_I = 40$ MeV, and $\mu_S = 125$ MeV.

in Fig. 6. For $q = 1.05$, the position of the CEP is approximately $(T, \mu) = (84$ MeV, 290 MeV$)$. A similar trend is shown in Fig. 7 for $q = 1.10$, where we found the CEP at approximately $(T, \mu)=(78$ MeV, 293 MeV$)$.

Figure 8 shows the deconfinement phase transition at $\mu_S = \mu_I = 0$ for different q values. This deconfinement phase transition remains a crossover over the entire range of the quark chemical potential. As the value of q increases, the phase transition temperature decreases to lower values. This means that with increasing non-extensivity, quarks can become deconfined even at lower temperatures. For $q = 1$, at zero chemical potential, the value of this temperature, T_d, is 164 MeV. This value decreases to $T_d = 153$ MeV for $q = 1.05$ and $T_d = 140$ MeV for $q = 1.10$. However, the decrease is less significant at a higher value of μ. For example, at $\mu = 350$ MeV, the values of T_d are observed to be 116, 111, and 105 MeV. This signifies that the impact of non-extensivity vanishes as we move towards lower temperatures. In Fig. 9 (a), the chiral phase transition of up and down quarks is shown for the q-PCQMF model in the $T - \mu$ plane for different values of q, at $\mu_S = \mu_I = 0$. For plotting the phase boundary in the crossover region, we used the maximum of χ_σ for a given value of μ, whereas, for the first-order transition, we used the maximum of χ_u for a given value of T. With an increase in non-extensivity of the system, the regime of first-order phase transition becomes smaller and the CEP is achieved at a higher value of μ and lower value of T. It is also clear from Fig. 9 (a) that the crossover transition, which occurs at higher temperatures, is distinctly different but the first-order phase transition, which occurs at lower temperatures is similar when $q > 1$. This is again evidence of the fact that non-extensivity vanishes at lower temperatures, i.e., $\Omega_q \to \Omega$ when $T \to 0$. The chiral phase transition of the s quark is shown in Fig. 9 (b) for $q = 1, 1.05,$ and 1.10. Contrary to the chiral phase transition of the u and d quarks, this phase transition remains a crossover over the entire range of the
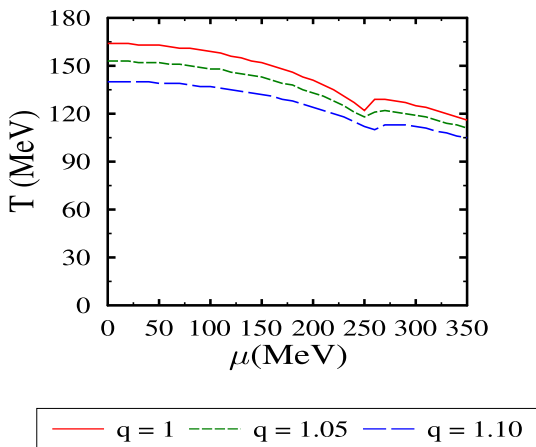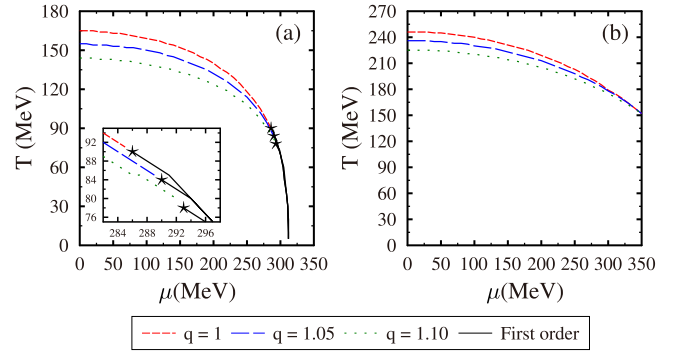

Fig. 9. (color online) Chiral phase transition for (a) u and d quarks and (b) s quark, at $\mu_S = \mu_I = 0$ MeV for $q = 1, 1.05,$ and 1.10.

$(T - \mu)$ phase diagram. Moreover, this phase transition also occurs at lower temperature values as q becomes greater than one. However, this difference in temperature at different q values disappears towards lower temperatures or higher chemical potentials, indicating the vanishing of non-extensive effects.

IV. SUMMARY AND CONCLUSIONS

We extended the PCQMF model to its non-extensive version and studied the properties of quark matter at finite temperature and density. We studied the thermodynamic properties and phase transitions with Tsallis statistics and compared the results with those obtained using the usual BG statistics. The non-extensivity was introduced in our model through the thermodynamic potential density, which modifies the form of the scalar and the vector densities of the quark resulting in the modification of the scalar, vector, and Polyakov loop fields. These modified fields are then further used to calculate various thermodynamic quantities. We found that quantities such as $\frac{\epsilon_q}{T^4}, \frac{p_q}{T^4}, \frac{s_q}{T^3},$ and $\frac{(\epsilon_q - 3p_q)}{T^4}$ all tend toward a new q-related Tsallis limit rather than their usual SB limit at high temperature for $q > 1$. We found that, as q increases, the criticality of c_{vq}/T^3 and c_{sq}^2 gradually decreases. In addition, the high-temperature limit of c_{sq}^2 is unaffected by the q parameter owing to a surprising cancellation [26]. Regarding the influence of the q parameter on the deconfinement phase transition, we found that this phase transition occurs at a lower value of T as the q parameter is increased. However, the nature of this phase transition is still a crossover, independent of q. Further, we studied the influence of the q parameter on the chiral phase transition for the u and d quarks as well as for the s quark. We found that, for the u and d quarks, the nature of this phase transition changes order from a crossover at high temperatures to a first-order phase transition at lower temperatures. Further, as q increases, the CEP is shifted towards a

Fig. 8. (color online) Deconfinement phase transition of quark matter at $\mu_S = \mu_I = 0$ MeV for $q = 1, 1.05,$ and 1.10.

lower T and a higher μ value. However, for the s quark, the phase transition remains a crossover but is shifted towards lower T values as q becomes greater than one. In addition, we found that the non-extensivity of the system disappears as we approach $T \to 0$. In the future, we aim to study the fluctuations and correlations of the conserved charges on the nuclear and hyperonic matter in the realm of non-extensivity.

APPENDIX A

The coupled equations are obtained by minimizing the thermodynamic potential density Ω_q with respect to the various fields of the q-PCQMF model and are given as

$$
\begin{aligned}
\frac{\partial \Omega_q}{\partial \sigma} =\ & k_0 \chi^2 \sigma - 4k_1 \left(\sigma^2 + \zeta^2 + \delta^2 \right) \sigma - 2k_2 \left(\sigma^3 + 3\sigma\delta^2 \right) - 2k_3 \chi \sigma \zeta - \frac{d}{3} \chi^4 \left(\frac{2\sigma}{\sigma^2 - \delta^2} \right) \\
& + \left(\frac{\chi}{\chi_0} \right)^2 m_\pi^2 f_\pi - \left(\frac{\chi}{\chi_0} \right)^2 m_\omega \omega^2 \frac{\partial m_\omega}{\partial \sigma} - \left(\frac{\chi}{\chi_0} \right)^2 m_\rho \rho^2 \frac{\partial m_\rho}{\partial \sigma} - \sum_{i=u,d} g_\sigma^i \rho_i^s = 0,
\end{aligned} \tag{A1}
$$

$$
\begin{aligned}
\frac{\partial \Omega_q}{\partial \zeta} =\ & k_0 \chi^2 \zeta - 4k_1 \left(\sigma^2 + \zeta^2 + \delta^2 \right) \zeta - 4k_2 \zeta^3 - k_3 \chi \left(\sigma^2 - \delta^2 \right) - \frac{d}{3} \frac{\chi^4}{\zeta} + \left(\frac{\chi}{\chi_0} \right)^2 \left[\sqrt{2} m_K^2 f_K - \frac{1}{\sqrt{2}} m_\pi^2 f_\pi \right] \\
& - \left(\frac{\chi}{\chi_0} \right)^2 m_\phi \phi^2 \frac{\partial m_\phi}{\partial \zeta} - \sum_{i=s} g_\zeta^i \rho_i^s = 0,
\end{aligned} \tag{A2}
$$

$$
\frac{\partial \Omega_q}{\partial \delta} = k_0 \chi^2 \delta - 4k_1 \left(\sigma^2 + \zeta^2 + \delta^2 \right) \delta - 2k_2 \left(\delta^3 + 3\sigma^2\delta \right) + 2k_3 \chi \delta \zeta + \frac{2}{3} d \chi^4 \left(\frac{\delta}{\sigma^2 - \delta^2} \right) - \sum_{i=u,d} g_\delta^i \rho_i^s = 0, \tag{A3}
$$

$$
\begin{aligned}
\frac{\partial \Omega_q}{\partial \chi} =\ & k_0 \chi \left(\sigma^2 + \zeta^2 + \delta^2 \right) - k_3 \left(\sigma^2 - \delta^2 \right) \zeta + \chi^3 \left[1 + \ln \left(\frac{\chi^4}{\chi_0^4} \right) \right] + (4k_4 - d)\chi^3 - \frac{4}{3} d\chi^3 \ln \left(\left(\frac{(\sigma^2 - \delta^2)\zeta}{\sigma_0^2 \zeta_0} \right) \left(\frac{\chi}{\chi_0} \right)^3 \right) + \\
& \frac{2\chi}{\chi_0^2} \left[m_\pi^2 f_\pi \sigma + \left(\sqrt{2} m_K^2 f_K - \frac{1}{\sqrt{2}} m_\pi^2 f_\pi \right) \zeta \right] - \frac{\chi}{\chi_0^2} (m_\omega{}^2 \omega^2 + m_\rho{}^2 \rho^2) = 0,
\end{aligned} \tag{A4}
$$

$$
\frac{\partial \Omega_q}{\partial \omega} = \frac{\chi^2}{\chi_0^2} m_\omega^2 \omega + 4g_4 \omega^3 + 12 g_4 \omega \rho^2 - \sum_{i=u,d} g_\omega^i \rho_i = 0, \tag{A5}
$$

$$
\frac{\partial \Omega_q}{\partial \rho} = \frac{\chi^2}{\chi_0^2} m_\rho^2 \rho + 4g_4 \rho^3 + 12 g_4 \omega^2 \rho - \sum_{i=u,d} g_\rho^i \rho_i = 0, \tag{A6}
$$

$$
\frac{\partial \Omega_q}{\partial \phi} = \frac{\chi^2}{\chi_0^2} m_\phi^2 \phi + 8g_4 \phi^3 - \sum_{i=s} g_\phi^i \rho_i = 0, \tag{A7}
$$

$$
\begin{aligned}
\frac{\partial \Omega_q}{\partial \Phi} =\ & \left[\frac{-a(T)\bar{\Phi}}{2} - \frac{6b(T)(\bar{\Phi} - 2\Phi^2 + \bar{\Phi}^2 \Phi)}{1 - 6\bar{\Phi}\Phi + 4(\bar{\Phi}^3 + \Phi^3) - 3(\bar{\Phi}\Phi)^2} \right] T^4 \\
& - \sum_{i=u,d,s} \frac{2k_B T N_C}{(2\pi)^3} \int_0^\infty \mathrm{d}^3 k \Bigg[\frac{e_q \left(\frac{-(E_i^*(k) - \nu_i^*)}{k_B T} \right)}{\left(1 + e_q \left(\frac{-3(E_i^*(k) - \nu_i^*)}{k_B T} \right) + 3\Phi e_q \left(\frac{-(E_i^*(k) - \nu_i^*)}{k_B T} \right) + 3\bar{\Phi} e_q \left(\frac{-2(E_i^*(k) - \nu_i^*)}{k_B T} \right) \right)^q} \\
& + \frac{e_q \left(\frac{-2(E_i^*(k) + \nu_i^*)}{k_B T} \right)}{\left(1 + e_q \left(\frac{-3(E_i^*(k) + \nu_i^*)}{k_B T} \right) + 3\bar{\Phi} e_q \left(\frac{-(E_i^*(k) + \nu_i^*)}{k_B T} \right) + 3\Phi e_q \left(\frac{-2(E_i^*(k) + \nu_i^*)}{k_B T} \right) \right)^q} \Bigg] = 0,
\end{aligned} \tag{A8}
$$

and

$$\frac{\partial \Omega_q}{\partial \bar{\Phi}} = \left[\frac{-a(T)\Phi}{2} - \frac{6b(T)(\Phi - 2\bar{\Phi}^2 + \Phi^2\bar{\Phi})}{1 - 6\bar{\Phi}\Phi + 4(\bar{\Phi}^3 + \Phi^3) - 3(\bar{\Phi}\Phi)^2} \right] T^4$$

$$- \sum_{i=u,d,s} \frac{2k_B T N_C}{(2\pi)^3} \int_0^\infty \mathrm{d}^3 k \left[\frac{e_q\left(\frac{-2(E_i^*(k) - \nu_i^*)}{k_B T}\right)}{\left(1 + e_q\left(\frac{-3(E_i^*(k) - \nu_i^*)}{k_B T}\right) + 3\Phi e_q\left(\frac{-(E_i^*(k) - \nu_i^*)}{k_B T}\right) + 3\bar{\Phi} e_q\left(\frac{-2(E_i^*(k) - \nu_i^*)}{k_B T}\right)\right)^q} \right.$$

$$\left. + \frac{e_q\left(\frac{-(E_i^*(k) + \nu_i^*)}{k_B T}\right)}{\left(1 + e_q\left(\frac{-3(E_i^*(k) + \nu_i^*)}{k_B T}\right) + 3\bar{\Phi} e_q\left(\frac{-(E_i^*(k) + \nu_i^*)}{k_B T}\right) + 3\Phi e_q\left(\frac{-2(E_i^*(k) + \nu_i^*)}{k_B T}\right)\right)^q} \right] = 0.$$

(A9)

References

[1] D. Boyanovsky *et al.*, Ann. Rev. Nucl. Part. Sci. **56**, 441 (2006)
[2] M. Buballa *et al.*, J. Phys. G **41**, 123001 (2014)
[3] G. Baym *et al.*, Rep. Prog. Phys. **81**, 056902 (2018)
[4] B.-L. Li *et al.*, Phys. Rev. D **99**, 043001 (2019)
[5] T. Hinderer *et al.*, Phys. Rev. D **81**, 123016 (2010)
[6] F. Weber, Prog. Part. Nucl. Phys. **54**, 193 (2005)
[7] R. Marty and J. Aichelin, Phys. Rev. C **87**, 034912 (2013)
[8] K. Tsushima *et al.*, Phys. Rev. C **59**, 2824 (1999)
[9] K. Saito and A.W. Thomas, Phys. Lett. B **327**, 9 (1994)
[10] B.J. Schaefer *et al.*, Phys. Rev. D **76**, 074023 (2007)
[11] T.K. Herbst *et al.*, Phys. Lett. B **696**, 58 (2011)
[12] D.P. Menezes *et al.*, J. Phys. G **32**, 1081 (2006)
[13] R. Stiele *et al.*, Phys. Lett. B **729**, 72 (2014)
[14] K. Fukushima, Phys. Lett. B **591**, 277 (2004)
[15] C. Ratti, M.A. Thaler, and W. Weise, Phys. Rev. D **73**, 014019 (2006)
[16] M. Abu-Shady and H. M. Mansour, Phys. Rev. C **85**, 055204 (2012)
[17] R. Gatto and M. Ruggieri, Phys. Rev. D **78**, 034015 (2011)
[18] B.J. Schaefer and M. Wagner, Prog. Part. Nucl. Phys. **62**, 381 (2009)
[19] P. Kovacs, Zs. Szep, and Gy. Wolf, Phys. Rev. D 93 **11**, 114014 (2016)
[20] P. Kovacs, G. Kovacs, and F. Giacosa, Phys. Rev. D 106 **11**, 116016 (2022)
[21] P. Wang *et al.*, Commun. Theor. Phys. **36**, 71 (2001)
[22] P. Wang *et al.*, Nucl. Phys. A **688**, 791 (2001)
[23] M. Kumari and A. Kumar, Eur. Phys. J. Plus **136**, 19 (2021)
[24] N. Chahal and A. Kumar, Chin. Phys. C **46**, 6 (2022)
[25] C. Tsallis, J. Stat. Phys. **52**, 479 (1998)
[26] Ya-Peng Zhao, Phys. Rev. D **101**, 096006 (2020)
[27] J. Rozynek and G. Wilk, Eur. Phys. A **52**, 13 (2016)
[28] T. Bhattacharyya *et al.*, Eur. Phys. J. A **52**, 30 (2016)
[29] Asmaa G. Shalaby, A. Phys. Pol. B **47**, 1301 (2016)
[30] G. Wilk and Z. Wlodarczyk, Eur. Phys. J. A **48**, 161 (2012)
[31] B.-C. Li, Y.-Z. Wang, and F.-H. Liu, Phys. Lett. B **725**, 352 (2013)
[32] L. Marques, J. Cleymans, and A. Deppman, Phys. Rev. D **91**, 054025 (2015)
[33] B. De, Eur. Phys. J. A **50**, 138 (2014)
[34] M. Rybczynski and Z. Wlodarczyk, Eur. Phys. J. C **74**, 2785 (2014)
[35] G. Combe *et al.*, Phys. Rev. Lett. **115**, 238301 (2015)
[36] U. Tirnakli and E. P. Borges, Sci. Rep **6**, 23644 (2016)
[37] L. J. L. Cirto, A. Rodriguez, F. D. Nobre *et al.*, EPL **123**, 30003 (2018)
[38] A. Adare *et al.* (PHENIX Collaboration),, Phys. Rev. C **83**, 064903 (2011)
[39] B. I. Abelev *et al.* (STAR Collaboration), Phys. Rev. C **75**, 064901 (2007)
[40] G. Aad *et al.* (ATLAS Collaboration), New J. Phys. **13**, 053033 (2011)
[41] K. E. A. Aamodt *et al.* (ALICE Collaboration), Eur. Phys. J. C **71**, 1655 (2011)
[42] V. E. A. Khachatryan *et al.* (CMS Collaboration), J. High Energy Phys. **02**, 041 (2010)
[43] I. Bediaga, E.M.F. Curado, and J.M. de Miranda, Physica A **286**, 156 (2000)
[44] W.M. Alberico, A. Lavagno, and P. Quarati, Eur. Phys. J. C **12**, 499 (2000)
[45] A. Lavagno, A.M. Scarfone, and P.N. Swamy, J. Phys. A **40**, 8635 (2007)
[46] C. Beck, Eur. Phys. J. A **40**, 267 (2009)
[47] G. Wilk and Z. Wlodarczyk, Phys. Rev. Lett. **84**, 2770 (2000)
[48] A. Lavagno and P. Quarati, Phys. Lett. B **498**, 47 (2001)
[49] T.S. Biro and G. Purcsel, Phys. Rev. Lett. **95**, 162302 (2005)
[50] T.S. Biro, G. Purcsel, and K. Urmossy, Eur. Phys. J. A **40**, 325 (2009)
[51] A. Lavagno, Phys. Lett. A **301**, 13 (2002)
[52] W.M. Alberico *et al.*, Physica A **387**, 467 (2008)
[53] P. Quarati and A.M. Scarfone, Astrophys. J. **666**, 1303 (2007)
[54] J.C. Carvalho *et al.*, Astrophys. J. **696**, L48 (2009)
[55] G. Livadiotis and D.J. McComas, Astrophys. J. **714**, 971 (2010)
[56] M.P. Leubner, Astrophys. J. **632**, L1 (2005)
[57] C. Tsallis, *Introduction to nonextensive statistical mechanics: approaching a complex world*, (Springer Science, 2009).

[58] F. I. M. Pereira, R. Silva, and J. S. Alcaniz, Phys. Rev. C **76**, 015201 (2007)
[59] J. Roynek and G. Wilk, J. Phys. G: Nucl. Part. Phys. **36**, 125108 (2009)
[60] P.H.G. Cardoso, T. Nunes da Silva, and A. Deppman *et al*., Eur. Phys. J. A **53**, 191 (2017)
[61] Ke-Ming Shen *et al*., Adv. High Energy Phys. **2017**(2017), 4135329 (2017)
[62] Ya-Peng Zhao *et al*., Chinese Phys. C **45**, 073105 (2021)
[63] Ya-Peng Zhao *et al*., Chinese Phys. C **47**, 053103 (2023)
[64] A. Drago, A. Lavagno, and P. Quarati, Physica A **344**, 472 (2004)
[65] A. Lavagno *et al*., J. Phys. G: Nucl. Part. Phys. **37**, 115102 (2010)
[66] A. Lavagno and D. Pigato, Eur. Phys. J. A **47**, 52 (2011)
[67] E. Megias, D. P. Menezes, and A. Deppman, Physica A **421**, 15 (2015)
[68] S.K. Tiwari *et al*., Eur. Phys. J. C **78**, 938 (2018)
[69] J. Schechter, Phys. Rev. D **21**, 3393 (1980)
[70] H. Gomm *et al*., Phys. Rev. D **33**, 801 (1986)
[71] E.K. Heide, S. Rudaz, and P.J. Ellis, Nucl. Phys. A **571**, 713 (1994)
[72] G. Carter, P.J. Ellis, and S. Rudaz, Nucl. Phys. A **603**, 367 (1996)
[73] P. Ko and S. Rudaz, Phys. Rev. D **50**, 6877 (1994)
[74] P. Papazoglou *et al*., Phys. Rev. C **59**, 411 (1999)
[75] P. Wang *et al*., Phys. Rev. C **67**, 015210 (2003)
[76] P. Wang *et al*., Nucl. Phys. A **705**, 455 (2002)
[77] P. Wang *et al*., Nucl. Phys. A **744**, 273 (2004)
[78] P. Costa *et al*., Symmetry **2**, 1338 (2010)
[79] S. Roessner *et al*., Phys. Rev. D **75**, 034007 (2007)
[80] S. Roessner *et al*., Nucl. Phys. A **814**, 118 (2008)
[81] M. Fukugita, M. Okawa, and A. Ukava, Nucl. Phys. B **337**, 181 (1990)
[82] D. H. E. Gross, Physica A **340**, 76 (2004)
[83] D. H. E. Gross, Physica A **365**, 138 (2006)
[84] J. Cleymans *et al*., Phys. Lett. B **723**, 351 (2013)
[85] M. D. Azmi and J. Cleymans, J. Phys. G **41**, 065001 (2014)
[86] T. Kodama *et al*., 2005 Europhys. Lett. **70**, 439 (2005)
[87] V. Garcia-Morales and J. Pellicer, Physica A **361**, 161 (2006)
[88] A. M. Teweldeberhan, A. R. Plastino, and H. C. Miller, Phys. Lett. A **343**, 71 (2005)
[89] T. S. Biro and A. Jakovac, Phys. Rev. Lett. **94**, 132302 (2005)
[90] A. Khuntia *et al*., Eur. Phys. J. A **52**, 292 (2016)
[91] H. Mao *et al*., J. Phys. G: Nucl. Part. Phys. **37**, 035001 (2010)